

Donor impurity in vertically-coupled quantum-dots under hydrostatic pressure and applied electric field

C.M. Duque¹, M.G. Barseghyan², and C.A. Duque^{1,a}

¹ Instituto de Física, Universidad de Antioquia, AA 1226, Medellín, Colombia

² Department of Solid State Physics, Yerevan State University, Al. Manookian 1, 0025 Yerevan, Armenia

Received 4 June 2009 / Received in final form 17 October 2009

Published online 17 December 2009 – © EDP Sciences, Società Italiana di Fisica, Springer-Verlag 2009

Abstract. In this work we make a predictive study on the binding energy of the ground state for hydrogenic donor impurity in vertically-coupled quantum-dot structure, considering the combined effects of hydrostatic pressure and in growth-direction applied electric field. The approach uses a variational method within the effective mass approximation. The low dimensional structure consists of three cylindrical shaped GaAs quantum-dots, grown in the z -direction and separated by $\text{Ga}_{1-x}\text{Al}_x\text{As}$ barriers. In order to include the pressure dependent $\Gamma-X$ crossover in the barrier material a phenomenological model is followed. The main findings can be summarized as follows: 1) for symmetrical and asymmetrical dimensions of the structures, the binding energy as a function of the impurity position along the growth direction of the heterostructure has a similar behavior to that shown by the non-correlated electron wave function with maxima for the impurity in the well regions and minima for the impurity in the barrier regions, 2) for increasing radius of the system, the binding energy decreases and for R large enough reaches the limit of the binding energy in a coupled quantum well heterostructure, 3) the binding energy increases for higher Aluminum concentration in the barrier regions, 4) depending of the impurity position and of the structural dimensions of the system (well width and barrier thickness) – and because changing the height of the potential barrier makes possible to induce changes in the degree of symmetry of the carrier-wave function –, the electric field and hydrostatic pressure can cause the impurity binding energy increases or decreases, and finally 5) the line-shape of the binding energy curves are mainly given by the line-shape of the Coulomb interaction.

1 Introduction

In recent years, based on the rapid progress in experimental crystal-growth techniques such as metal-organic chemical-vapor deposition, liquid-phase epitaxy, and molecular-beam epitaxy, the external hydrostatic pressure effects on impurity states of low-dimensional systems have received increased attention both theoretically and technologically. These new crystal-growth techniques open up opportunities to study the optoelectronic properties and band structure of semiconductor superlattices and heterostructures under hydrostatic pressure, including coupling effects, resonant tunneling effects, and polarizability phenomena. It is now known that these effects can be enhanced under hydrostatic pressure, a fact which may lead to many potential applications in optoelectronic devices [1–6], such as strained semiconductor quantum well lasers, transducers, infrared detectors, resonant tunneling diodes, and ballistic transistors. Many theoretical investigations have been reported concerning the effects of hydro-

static pressure on shallow-donor impurity states in GaAs- $\text{Ga}_{1-x}\text{Al}_x\text{As}$ quantum wells (QW) [7–12], quantum-well wires (QWW) [13–15] and quantum dots (QD) [16–19]. In the case of vertically coupled GaAs- $\text{Ga}_{1-x}\text{Al}_x\text{As}$ QDs, the combined effect of hydrostatic pressure and magnetic field has also been considered [20]. In addition, effects of hydrostatic pressure on both electrical and transport properties of two-dimensional electron gas in delta-doped systems have been reported in recent years [21–24]. The $\Gamma-X$ crossover for the barrier material in multiple quantum well (MQW) structures was observed experimentally by Venkateswaran et al. [25] and Burnett et al. [26] who studied the pressure dependence of photoluminescence spectra in such systems. The $\Gamma-X$ crossover has been theoretically studied [7–9,19] and, as a general feature, the researchers have found a linear dependence on the binding energy in the direct-gap regime under the applied pressure, while in the indirect-gap regime (applied pressure larger than 13.5 kbar) the energy grows with the pressure until a maximum is reached, and then it decreases. Additionally, they have shown a red-shift in the shallow-donor-related optical-absorption spectra associated mainly with

^a e-mail: cduque@fisica.udea.edu.co

the pressure dependence of the band gap of the well material. In almost all the references cited above the general characteristic is the effective mass approximation and the use of variational techniques.

The application of an electric field along the growth direction of the heterostructure gives rise to a polarization of the carrier distribution and to an energy shift of the quantum states. Such effects may introduce considerable changes in the energy spectrum of the carriers, which could be used to control and modulate the output of optoelectronic devices. Simultaneous effects of hydrostatic pressure and electric field on shallow donor impurity states in QW have been investigated by Morales et al. [27]. For low-pressure regime these authors observed a linear binding energy behavior, whereas for high pressure the simultaneous effects of both the barrier height and the applied electric field bend the binding energy curves towards smaller values. For the range of low hydrostatic pressure they observed that the impurity polarization remains constant in all cases but it increases as the field goes up. Morales et al. [28] and Kasapoglu [29] have reported the combined effect of hydrostatic pressure and electric field on the binding energy of a shallow-donor impurity in a double QW. Results for the binding energy as a function of the applied electric field, for fixed values of pressure, show strong changes for fields smaller than 20 KV/cm and a softer behavior for larger fields. In the work reported by Bai et al. [30] the effects of hydrostatic pressure on the binding energies of shallow-donor impurity states in double QWW are studied. As a general feature, the authors observed that, for various positions of the donor ion and for fixed pressure values the coupling effects become stronger when the barrier widths become smaller. On the other hand there is increasingly strong coupling with increasing applied pressure for the same barrier widths. Also, Bai et al. [30] studied the binding energy of the ground state of shallow-donor impurity, with respect to the first subband, in vertically coupled QDs. The variation of the ground-state binding energy of an impurity located at the center of the inner dot was considered as a function of the width of a dot as well as the thickness of the barrier in the z -direction. All the behaviors of the binding energy are resolved by the competition between the wave function localization effect and the wave function tunneling effect. The effects of hydrostatic pressure on the binding energy of shallow-donor impurity states in double QD have been calculated by Liu et al. [31]. The pressure dependence of the binding energy for different donor ion positions has been reported in that paper: for pressure values up to 13.5 kbar, the binding energy increases linearly with the pressure; for pressure values greater than 13.5 kbar, the direct gap regime passes into the indirect-gap regime, where the $\Gamma - X$ crossover in the barrier material reduces the barrier height with increasing pressure, causing the non-linear variation on the binding energy.

Semiconductor QDs are human-made nanostructures in which the carriers, i.e., electrons and holes, are confined in all spatial directions. In that respect, therefore, such QDs are often referred to as “artificial atoms” as they

show typical atomic properties like discrete energy levels and shell structures. Starting from QDs as a nanostructure, more developed and complex systems are conceivable; they are promising in future device applications. A trivial example is the analogy of a two-atom molecule with a semiconductor nanostructure consisting of two coupled QDs, in which one may think of the QD coupling as being either vertical, lateral, or both simultaneously.

Time-resolved photoluminescence measurements in single period laterally coupled QD and multiple period vertically stacked QD have been made by Neogi et al. [32]. They observed that at low temperatures the recombination time in single coupled QDs is over an order of magnitude longer than the nonradiative recombination process at 100 K, and that the vertical correlation among the adjoining stacked layer leads to an enhancement of the photoluminescence efficiency in multiple period QDs and results in an efficient emission at room temperature. They also found that the binding energies in multiple period QDs are stronger by more than six times compared to single period QDs. Lateral quantum coupling between two self-assembled (In,Ga)As QD has been confirmed by photon statistics measurements; this could be understood as a displayed strong antibunching between the various excitonic and biexcitonic transitions of these lateral QD molecules [33]. Also, the direct observation of quantum coupling in individual QD molecules and its manipulation using static electric fields has been reported by Krenner et al. [34].

On the other hand, the fabrication of a strain-free, laterally aligned GaAs/Al_{0.27}Ga_{0.73}As QD pair structure using droplet epitaxy has been demonstrated by utilizing the anisotropic surface potentials of the GaAs (100) surface [35]. The micro-photoluminescence spectra of a single QD pair shows an ensemble of emissions which may indicate the existence of a tunnel coupling between the QDs.

The effects of an applied electric field on the exciton spectra in vertically coupled QD have been carefully studied by Szafran and co-workers [36–40]. They considered in detail the intermediate- and strong-coupling regimes and they explained how the spectra evolves when an extra dot is added to the stack. Also, they have shown that for vertically coupled dots their imperfect alignment does not qualitatively influence the exciton Stark effect of the electric field oriented in the growth direction and that the deviations from the quadratic Stark effect are due to energy levels crossings (or very narrow avoided crossings). Zheng [41] has reported a theoretical study of the binding energy of a donor-impurity in cylindrical-shape multiple QD heterostructures (MQD), showing that the binding energy is strongly dependent on the quantum dot size. Magnetic field effects and single electron states in vertically coupled QDs have been also reported [42–44].

The present work is concerned with the theoretical study of a donor impurity in a multiple GaAs-Ga_{1-x}Al_xAs QD under the combined effects of an electric field applied in the growth-direction, and hydrostatic pressure. The effective-mass and parabolic band approximations have been considered within the variational procedure.

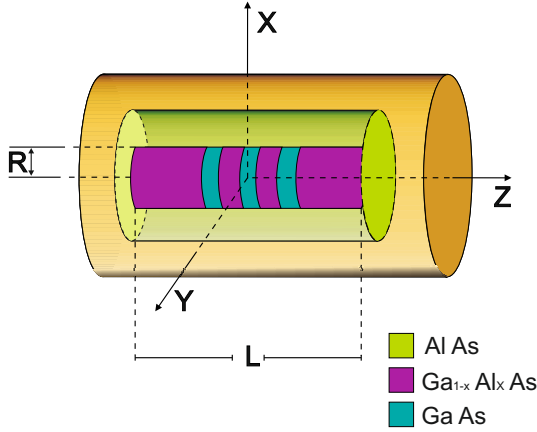


Fig. 1. (Color online) Pictorial view of the MQD system studied in the present work.

The paper is organized as follows. In Section 2 we describe the theoretical status of the discipline. Section 3 is dedicated to the results and discussion, and finally, our conclusions are given in Section 4.

2 Theoretical framework

Here we are concerned with the donor-impurity states in GaAs-Ga_{1-x}Al_xAs MQD grown along the z -axis in the presence of growth-direction electric field ($\mathbf{E} = -E\hat{z}$) and under the effects of hydrostatic pressure (P). In Figures 1 and 2 we present a pictorial view of the cylindrical-shape MQD that we are considering in this work. The material for the potential barriers in the axial and radial directions are, respectively, Ga_{1-x}Al_xAs (with x labeling the Aluminum molar fraction) and AlAs. Here, we have considered that the confinement on the electrons is due to the difference of the bandgaps in the Γ -point of the first Brillouin's zone, taking into account the appropriate band-offsets. The dimensions along the z -direction of the well and barrier regions have been defined. Figure 2 also shows three particular donor-impurity positions (in the center of each QD), the applied electric field, and the barrier confinements along the growth-direction. The infinite barrier QW, whose size is L , is used in the work in order to obtain the non correlated electron wave function along the z -direction [45]. From now on the dimensions of the MQD heterostructure will be always referred as $(L_{QD1}, L_{DQ2}, L_{QD3}, L_{B1}, L_{B2}, R)$. Also, the three QDs will be referred as QD1, QD2, and QD3 (see Fig. 2). The present theoretical approach uses the envelope-function and parabolic-band approximations [46,47]; so, the Hamiltonian for the donor-impurity, in cylindrical coordinates, takes the following form [41,48–50]

$$H = -\frac{\hbar^2}{2m^*(P)} \left(\frac{\partial^2}{\partial \rho^2} + \frac{1}{\rho} \frac{\partial}{\partial \rho} + \frac{1}{\rho^2} \frac{\partial^2}{\partial \phi^2} + \frac{\partial^2}{\partial z^2} \right) + V(\rho, z, P) - |e| E z - \frac{e^2}{\varepsilon(P) \sqrt{\rho^2 + (z - z_0)^2}}, \quad (1)$$

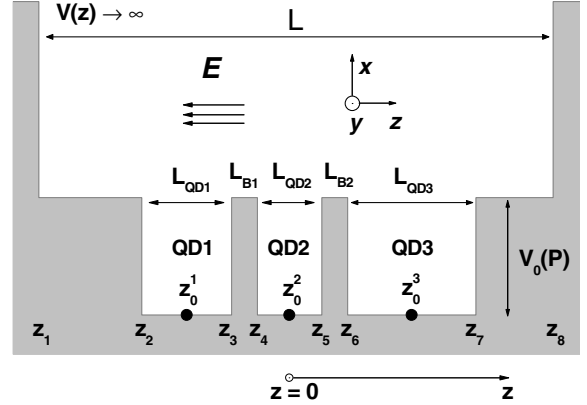


Fig. 2. (Color online) Pictorial view of the hydrostatic pressure dependent z -direction confinement potential for the MQD system studied in the present work. The quantum dot lengths, the barriers thickness, and the infinite-barrier quantum well width, used to model the electron wave function, are depicted. The direction of the applied electric field, three particular positions of the impurity along the z -direction ($z_0^i, i = 1, 2, 3$), and the axial positions of the different interfaces in the MQD ($z_i, i = 1, 2, 3, \dots, 8$), are showed as well.

where (ρ, z) and $(0, z_0)$ are the electron and impurity coordinates, e is the the electron charge, and $m^*(P)$ and $\varepsilon(P)$ are the hydrostatic pressure-dependent electron effective mass and static dielectric constant, respectively (for simplicity, the dielectric constant and the effective masses are considered to be the same as in GaAs throughout the GaAs-Ga_{1-x}Al_xAs MQD). $V(z, \rho, P) = V(z, P) + V(\rho, P)$ are the hydrostatic pressure-dependent MQD confining potentials with

$$V(\rho, P) = \begin{cases} 0, & \text{if } \rho \leq R, \\ \infty, & \text{if } \rho \geq R, \end{cases} \quad (2)$$

$$V(z, P) = \begin{cases} \infty, & \text{if } z < z_1, \\ V_0(P), & \text{if } z_1 \leq z < z_2, \\ 0, & \text{if } z_2 \leq z < z_3, \\ V_0(P), & \text{if } z_3 \leq z < z_4, \\ 0, & \text{if } z_4 \leq z < z_5, \\ V_0(P), & \text{if } z_5 \leq z < z_6, \\ 0, & \text{if } z_6 \leq z < z_7, \\ V_0(P), & \text{if } z_7 \leq z \leq z_8, \\ \infty, & \text{if } z > z_8. \end{cases} \quad (3)$$

From equation (2), it is clear that in our model we are approaching to infinite the potential barriers in the radial direction due to the presence of the AlAs material. In other words, this limit of the potential barrier in the radial direction is equivalent to consider, for example, a GaAs-vacuum interface instead of considering a GaAs-AlAs interface.

In order to obtain the impurity eigenfunctions for the GaAs-Ga_{1-x}Al_xAs DQW, we adopt the variational

scheme used by Fox *et al* [51] and Galbraith and Duggan [52] which consists of minimizing the functional

$$E(\Phi) = \langle \Phi | \hat{H} | \Phi \rangle \quad (4)$$

using the variational wave functions as

$$\Phi(\rho, z) = f(z) J_0(k_{10}\rho) e^{-\lambda r}, \quad (5)$$

where $f(z) J_0(k_{10}\rho)$ [J_0 is the ordinary Bessel's function with $J_0(k_{10}R) = 0$] is the eigenfunction (with eigenvalue E_0) of the Hamiltonian in equation (1) without the impurity potential term at the right and λ is a variational parameter. We note that the non-correlated function $f(z)$ is readily obtained via the method of Xia and Fan [45] which consists of an expansion in terms of sine functions associated with the infinite barrier QW of width L . For the applied electric field values reported in this study – less than 100 kV/cm –, the electron-impurity system always corresponds to a bound problem. That is the reason for which the model of the trial wave function that we used is a correct choice to describe the Stark effect [53,54]. Even in the case of very strong electric fields, due to the infinite potential barriers in $\pm L/2$, considered in the model, one always obtain a bound state for the ground energy of the electron-impurity system. For the GaAs electron effective mass and the static dielectric constant we have used [1,55,56], respectively:

$$m^*(P) = \left[1 + \frac{15020 \text{ meV}}{E_g(P)} + \frac{7510 \text{ meV}}{E_g(P) + 341 \text{ meV}} \right]^{-1} m_0, \quad (6)$$

and

$$\varepsilon(P) = 12.58 \exp(-1.67 \times 10^{-3} \text{ kbar}^{-1} P), \quad (7)$$

where $E_g(P)$ is the bulk GaAs bandgap

$$E_g(P) = (1519 + 10.7 \text{ kbar}^{-1} P) \text{ meV}, \quad (8)$$

m_0 is the free electron mass, and x is the alloy concentration.

Here we follow the model of Elabsy [7] in which the $\Gamma - X$ crossover in the $\text{Ga}_{1-x}\text{Al}_x\text{As}$ material, which is induced by the effect of hydrostatic pressure, is introduced into the model through the pressure dependence of the height of the barrier that confines the electrons in the z -direction. In particular, for pressures below ~ 13.5 kbar [7,26] the height of the barrier remains constant while for pressures larger than this value the height of the barrier decreases with pressure. The parameters that describe the dependence of the barrier height with the hydrostatic pressure are obtained from fittings with experimental results of the photoluminescence-peak energy transition in semiconductor heterostructures. So, for the MQD confined potential along the z -direction we have used [7]

$$V_0(P) = \begin{cases} \Gamma_b^{(P)} - \Gamma_w^{(P)}, & P \leq P_1, \\ X_b^{(P)} - \Gamma_w^{(P)} + S_0 x \frac{P-P_1}{P}, & P_1 < P \leq P_2 \end{cases} \quad (9)$$

here P_1 (13.5 kbar) is the crossover pressure between the $X_b^{(P)}$ - and the $\Gamma_b^{(P)}$ -conduction bands for the barrier material, and P_2 (35 kbar) is the crossover pressure between the $X_b^{(P)}$ -conduction band in the barrier and the $\Gamma_w^{(P)}$ -conduction band in the well. S_0 (250 meV) [7] is an adjustable parameter used to fit the predicted energy at P_1 with the experimental result. Finally, the pressure dependent well-width and barrier-width ($L_i(P)$) are obtained from

$$L_i(P) = L_i(P=0) [1 - (S_{11} + 2S_{12})P], \quad (10)$$

where $S_{11} = 1.16 \times 10^{-3} \text{ kbar}^{-1}$ and $S_{12} = -3.7 \times 10^{-4} \text{ kbar}^{-1}$ are the compliance constants of bulk GaAs [1,57,58] and $L_i(P=0)$ corresponds to the well- or barrier-width at $P=0$.

3 Results and discussion

In Figure 3 we present our results for the binding energy of a donor impurity in a vertically $\text{GaAs-Ga}_{1-x}\text{Al}_x\text{As}$ MQD as a function of the impurity position along the growth direction of the structure. We have considered two different structures: in the first structure (Fig. 3a), due to the symmetry of the potential, the binding energy is also symmetric with respect to $z=0$. In the second structure (Fig. 3b), the potential is slightly asymmetric, and correspondingly, the symmetry in the binding energy is broken. Let us concentrate on Figure 3a. The binding energy shows a maximum at the center of each well and minima at the barrier regions. As the impurity gets closer to the barriers, the binding energy diminishes, because the barriers repel the wave function and polarize the electron-impurity system, thus causing an increase in the expectation value of the z -distance between them, $\langle |z - z_0| \rangle$, with a consequent decrease in the Coulomb interaction. As the Aluminum concentration increases – dashed line in Figure 3a – the height of the barriers increases, forcing the probability of finding the carriers in the region of the barriers to decrease, with a corresponding increase of the probability in the well regions. Thus, when the Aluminum concentration increases, the binding energy decreases for impurities in the barriers and increases for impurities in the wells. When considering structures where the wells have different widths (Fig. 3b), it is clear that the probability of finding the electron is higher in the well of greater width and decreases towards the regions of lower well widths, as shown by the solid line in Figure 3d. By moving the impurity along the growth-direction, it is clear that when it is in the region of the QD1 the binding energy reaches a highest value, since $\langle |z - z_0| \rangle$ is at its minimum possible value ($\sim 40 \text{ \AA}$), as shown by the solid line in Figure 3c. By moving the impurity to the QD2 the binding energy naturally decreases, because $\langle |z - z_0| \rangle = 120 \text{ \AA} \sim L_{QD1}/2 + L_{B1} + L_{QD2}/2 = 137.5 \text{ \AA}$, with a corresponding decrease in the Coulomb interaction (see Fig. 3c). When the impurity is located at the center of the QD3 the binding energy keeps declining because now $\langle |z - z_0| \rangle = 241 \text{ \AA}$

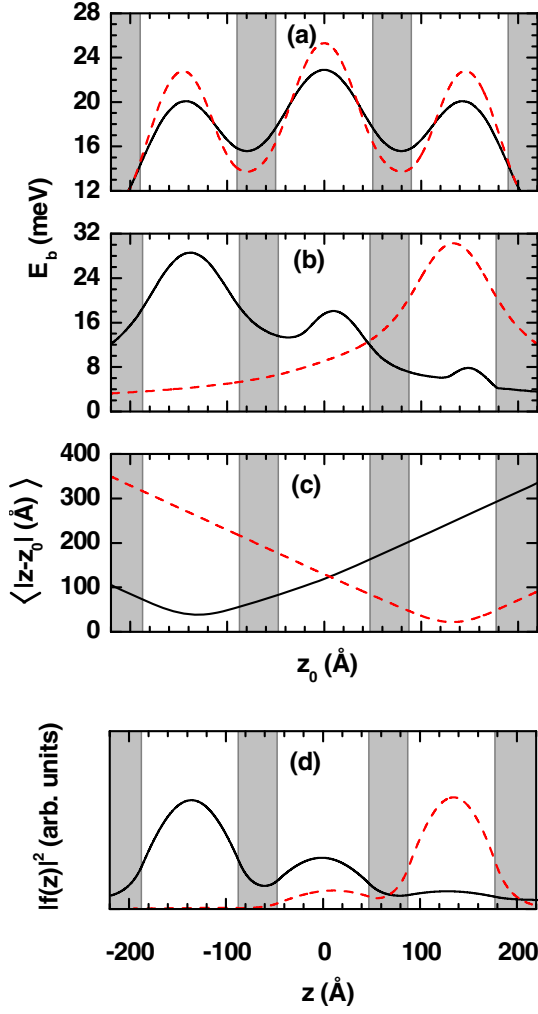


Fig. 3. (Color online) Binding energy of a donor impurity in cylindrical-shape vertically coupled GaAs-Ga_{1-x}Al_xAs MQD as a function of the impurity position along the z -direction (a, b). The dimensions of the structure are (100, 100, 100, 40, 40, 100) Å (a) and (100, 95, 90, 40, 40, 100) Å (b). In (a) $F = 0$ and solid lines are for $x = 0.1$ whereas dashed lines are for $x = 0.3$. In (b) $x = 0.3$ with $F = 0$ for solid lines and $F = 8$ kV/cm for dashed lines. In (c) and (d) the results are for the same configuration as in (b) but, respectively, for the expectation value of the electron-impurity distance, in the z direction, as a function of the z_0 -impurity position and for the probability density, along the z -direction, for the ground state of electrons in the heterostructure without consider the Coulomb interaction.

or $\sim L_{QD1}/2 + L_{B1} + L_{QD2} + L_{B2} + L_{QD3}/2 = 225.5$ Å (see Fig. 3c). When the electric field is applied in the $-z$ -direction, there is a force on the electrons in the $+z$ -direction; correspondingly, the probability of finding the electrons in the QD1 decreases, and the probability in the QD3 increases (see dashed curve in Fig. 3d). The shape of the binding energy curve in Figure 3b is essentially asymmetric; but it may be artificially symmetrized if we apply a suitable electric field. Now, when the impurity is shifted from the center of the QD1 to the center of

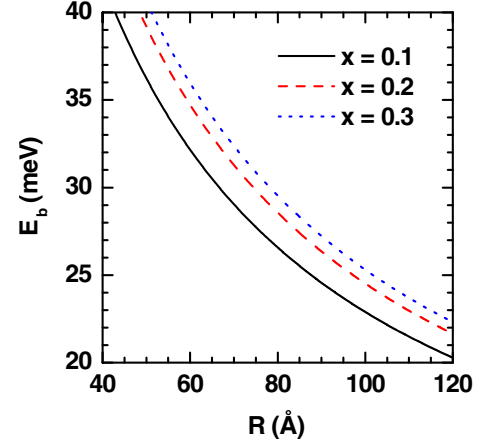


Fig. 4. (Color online) Binding energy of a donor impurity in cylindrical-shape vertically coupled GaAs-Ga_{1-x}Al_xAs MQD as a function of the radius of the structure. The dimensions of the structure are taken as (100, 100, 100, 40, 40, R) Å with $z_0 = z_0^2$ and considering different values of Aluminum concentration.

the QD2, the expectation value $\langle z - z_0 \rangle$ diminishes from 170 Å $\sim L_{QD1}/2 + L_{B1} + L_{QD2} + L_{B2} + L_{QD3}/2$ to 23 Å (see the dashed line in Fig. 3c). This occurs with a corresponding increase in the binding energy, which is represented by the dashed curve in Figure 3b.

In Figure 4 we present our results for the binding energy as a function of the radius of a system of three vertically GaAs-Ga_{1-x}Al_xAs MQD. As the radius increases the binding energy decreases because the wave function of the system is spreading over a larger transverse region of the MQD system, with a corresponding increase in the expectation value of the in-plane electron-impurity distance, $\langle \rho \rangle$. For sufficiently large radii our results reproduce the exact value of the three coupled QWs system. When the radius of the structure goes to zero the binding energy increases monotonically, due to the infinite barriers in the radial direction. It is clear that an increasing of the Aluminum concentration (by comparing the solid, dashed, and dotted line curves) should increase the binding energy because, in addition to the radial confinement, we now must add a higher confinement along the z -direction.

In Figure 5 we present our results for the binding energy of a donor impurity in a GaAs-Ga_{1-x}Al_xAs MQD as a function of the length of the dots and thickness of the barriers; we study those cases in which both length and thickness increase in the same proportion. Since in our calculations we have taken a typical value $L = 600$ Å, the maximum value of the length of each dot and/or thickness of each barrier is $600/5$ Å = 120 Å; this corresponds to the maximum value reported on the horizontal axis in Figure 5. Note (see Fig. 2) that when the length of the dots and/or barriers is zero, the impurity-electron system is confined in a Ga_{1-x}Al_xAs QD surrounded by infinite barriers both in the z and ρ directions. In this case the system is in the minimum value of the confinement effect because the barriers and the binding energy correspond essentially to a system confined in a single QD of radius 100 Å. Although it is not shown here, it is important to

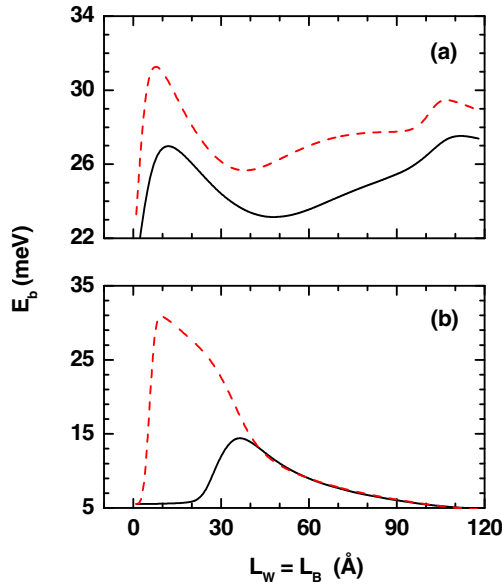


Fig. 5. (Color online) Binding energy of a donor impurity in cylindrical-shape vertically coupled GaAs-Ga_{1-x}Al_xAs MQD as a function of the well=barrier width of the structure for $R = 100$ Å and $z_0 = z_0^*$. Solid lines are for $x = 0.1$ and dashed lines for $x = 0.3$. In (a) $F = 0$ whereas in (b) $F = 30$ kV/cm.

clarify that in the limit when both length and thickness are zero, the two curves – solid and dashed – go exactly to the same binding energy value; this is consistent with the fact that in this limit the binding energy only depends on R and L but not on the Aluminum concentration, due to the absence of finite potential barriers. When the length of the dots and the thickness of the barriers acquire a finite value δ , slightly greater than zero, the system is immediately confined in a quantum dot of radius 100 Å and length 3δ since in that range the three quantum dots are strongly coupled. Note that in the small length range the binding energy is of the order of $4R^*$, which corresponds to a 2-dimensional hydrogenic atom. As the z dimensions grow the system loses confinement in z -direction, and thus should present a decrease in the binding energy, as observed in both curves in Figure 5a in the range between 20 Å and 50 Å, approximately. From 50 Å, the thickness of the barriers begins to decouple the QDs and thus the binding energy starts to increase; this happens because the system is essentially confined in the QD2 region, where the impurity is located. Additionally, in this range the infinite barriers at $\pm L/2$, begin to exert their effect because the dimensions of our structure begin to reach the limits of saturation. The results of increasing the Aluminum concentration (comparing the dashed to the solid lines) show a similar behavior but with larger binding energy corresponding to the presence of a higher potential barrier in the z -direction. An applied electric field dramatically changes the behavior of the binding energy. In the limit of small width we essentially obtain a strongly polarized hydrogenic atom since the wave function is oriented towards the infinite wall at $z = +L/2$ and the expectation value of z -distance between the elec-

tron and the impurity is of the order of 300 Å; this comes accompanied with a small value in the binding energy. When the length/thickness is of the order of 10 Å, the system is essentially confined into a QD of length 30 Å because the three dots are strongly coupled among themselves. Here a low Aluminum concentration, as in the solid line, cannot confine the system in the QDs regions and therefore the binding energy remains essentially constant. But at sufficiently high Aluminum concentration, $x = 0.3$, the barriers are high too; in these conditions the binding energy grows steeply to a maximum (see the dotted line in Fig. 5b), in spite of the presence of the electric field. For low Aluminum concentrations (solid line) we also obtain the same dramatic growth of the binding energy, but in a larger QD length. Having a larger available space, the wave function spreads, thus facilitating the polarization of the system; this comes accompanied with a decrease in the binding energy: this happens after the binding energy reaches a maximum and starts to decrease.

Figure 6 shows the dependence with the applied electric field of the binding energy for a donor impurity in a system of vertically coupled MQD of lengths 100 Å, 80 Å and 60 Å for L_{QD1} , L_{QD2} , and L_{QD3} respectively. Two positions of the impurity have been considered. Note, Figure 6c, that without impurity and at 4 kV/cm the probability of finding the electron in QD1 is maximum, very low in QD2, and almost zero in QD3. This situation is almost the same at zero field, implying that the effect of the field at 4 kV/cm is negligible. When considering an electric field of 12 kV/cm the probability is maximum in QD2 and very low in QD1 and QD3. For a field of 24 kV/cm the electron is essentially located in QD3. Let us now consider the effect of the impurity, when it is located at the center of the QD2 (Fig. 6a); note that at low fields the z -distance between the electron and the impurity is of the order of the distance between the QD1 and QD2. By increasing the field, this distance is of the order of 0, with the corresponding increase in the binding energy, as shown by solid and dashed curves in Figure 6a. If now the field continues to grow, the expectation value of the z -distance increases again to a value of the order of the distance between the QD2 and the QD3, with the corresponding decrease in the binding energy. Note that the QD1-QD2 distance is greater than the QD2-QD3 distance and thus, in the low field limit, the binding energy value is smaller than the binding energy for the high fields limit, as we observe by the dotted line. At low Aluminum concentration (solid line) the curve shows a similar behavior, but not as well defined like the one we obtained for high concentrations. Now we go to the impurity at the center of the QD3 (Fig. 6b). In this case, the expectation value of the z -distance evolves from the QD1-QD3 distance, through QD2-QD3, and ends at approximately zero. That means that at any time the binding energy presents an increasing behavior. For high Aluminum concentrations, this behavior has the shape of “steps” appearing in the dashed line in Figure 6b. A possible explanation is as follows: in the low field range, from 0 to 8 kV/cm, the electron is essentially located in the QD1; for fields between 8 kV/cm

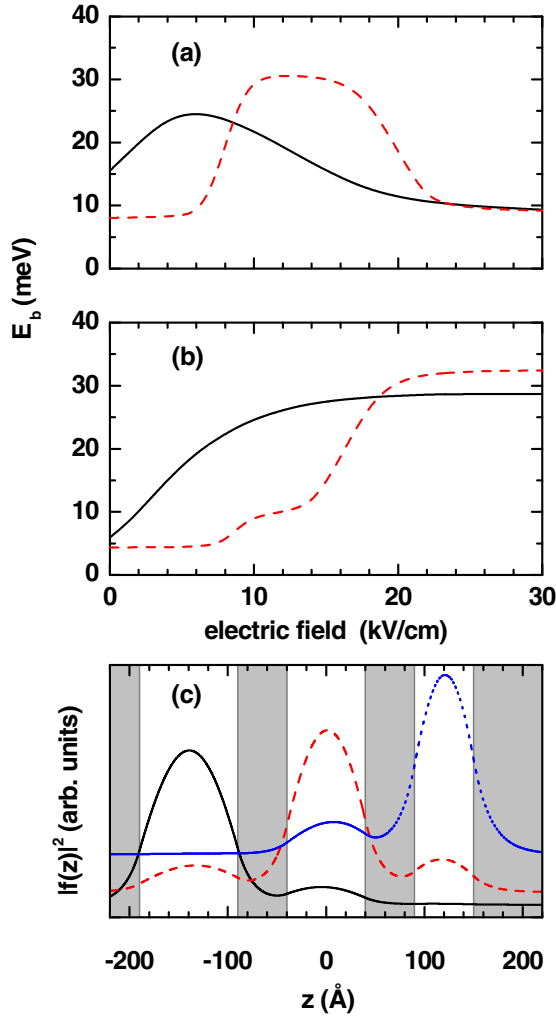


Fig. 6. (Color online) Binding energy of a donor impurity in cylindrical-shape vertically coupled GaAs-Ga_{1-x}Al_xAs MQD as a function of the in-growth direction applied electric field (a, b). The dimensions of the structure are (100, 80, 60, 50, 50, 100) Å. In (a) $z_0 = z_0^2$ whereas in (b) $z_0 = z_0^3$. Solid and dashed lines are for $x = 0.1$ and $x = 0.3$, respectively. In (c) the results are for the same dimensions of the structure and $x = 0.3$, but for the probability density along the z -direction for the ground state of the electrons in the heterostructure without considering the Coulomb interaction. Solid, dashed, and dotted lines are, respectively, for 4 kV/cm, 12 kV/cm, and 24 kV/cm of the applied electric field.

and 14 kV/cm the electron passes to the QD2 region, and finally at fields greater than 20 kV/cm, it is essentially located in the QD3. For low barriers, solid line, note that the transition between the QD1 and QD3 regions is made in a soft way, which reflects the low value of the geometric confinement in the z -direction.

In Figures 7a and 7b we present our results for the binding energy of a donor impurity in a coupled MQD system as a function of the hydrostatic pressure, for two different values of applied electric field. The results are presented for impurities located at the centers of each QD that form the structure. The dimensions of the structure

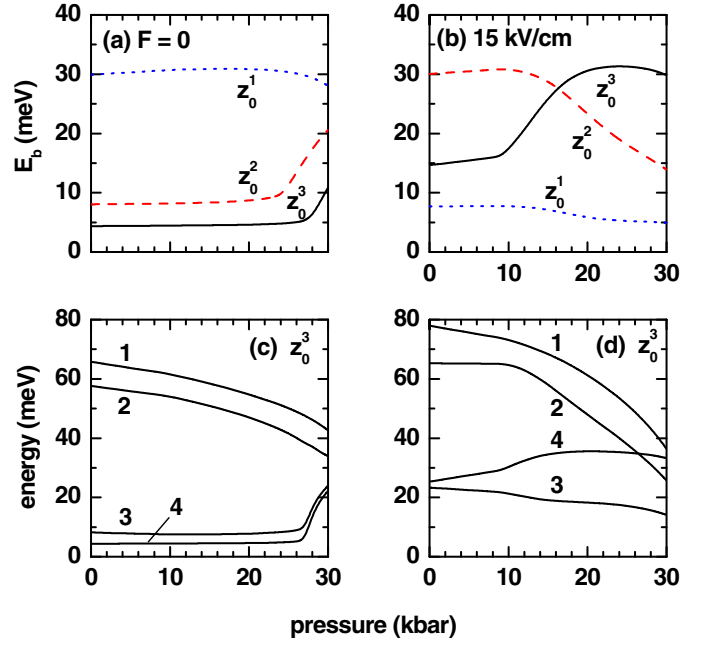


Fig. 7. (Color online) (a,b) Binding energy of a donor impurity in cylindrical-shape vertically coupled GaAs-Ga_{1-x}Al_xAs MQD as a function of the hydrostatic pressure. The dimensions of the structure are (100, 80, 60, 50, 50, 100) Å with $x = 0.3$. In (a) $F = 0$ whereas in (b) $F = 15$ kV/cm. Solid, dashed, and dotted lines are, respectively, for $z_0 = z_0^3$, $z_0 = z_0^2$, and $z_0 = z_0^1$. (c,d) The different energies associated with the four terms at the right side of equation (1): term 1+term 2+term 3 (E_0 – line 1), term 1 (E_{kinetic} – line 2), term 2 ($E_{\text{confinement}}$ – line 3), and absolute value of term 4 ($|E_{\text{Coulomb}}|$ – line 4). The results are for the impurity at z_0^3 with the same dimensions considered for Figures (a) and (b). In (c) $F = 0$ whereas in (d) $F = 15$ kV/cm.

are the same as the ones presented in Figure 6; and thus Figure 6c is useful for the discussion of Figure 7. In the case of Figure 7a and in accordance with the solid line in Figure 6c, the probability of finding the electron along the z direction is maximum in the region of the QD1. Consequently, when the impurity is moved from QD3 to QD2 and finally to QD1, the expectation value of the z -distance between the electron and the impurity decreases. This, in turn, comes accompanied with an increasing in the binding energy, as we pass from the solid line to the dashed line and finally to the dotted line in Figure 7a. For impurities in QD2 and QD3 the binding energy is essentially constant over the pressure regime in which the height of the barrier is high enough to allow the electron wave function to remain mainly distributed along QD1. With an increasing pressure in the regime of the $\Gamma - X$ crossover for the barrier material, we have a reduction in the height of the barriers and hence the electronic wave function starts to spread around the center of QD2, with the corresponding decreasing in the expectation value of z -distance and the increasing in the binding energy, as it is shown in the upward bending of the solid and dashed curves. In the case of an impurity in QD1, the behavior

is as follows. Initially, $\langle |z - z_0| \rangle$ is close to zero and therefore the binding energy is at its maximum. As the pressure increases, there is a decreasing in the dielectric constant, so we have an increasing of the Coulomb interaction with the corresponding quasi-linear increasing of the binding energy. When the $\Gamma - X$ crossover appears, near to $P = 12$ kbar, the height of the barrier begins to fall and then the binding energy reaches a maximum. Finally it decreases to a value that is similar to the one obtained for impurities at QD2 and QD3. Now, turning to Figure 7b, where there is a field of 15 kV/cm, it is clear that the electron wave function is essentially about the QD2 and decreases towards QD1 and QD3. In this case, when the impurity is located at QD2 and in the zero pressure limit, the binding energy must be comparable to the value obtained with zero field and with the impurity in QD1 (compare dotted line in (a) with dashed line in (b)). Note that now, at zero pressure and for the impurity at QD1, the binding energy is lower than in Figure 7a (compare the two dotted lines in (a) and (b)) and for QD3 is higher than in Figure 7a (compare the two solid lines in (a) and (b)). With an increasing in the pressure the height of the barriers decreases so now the electric field is large enough to make the probability of finding the electron along the z -direction maximum in QD3, and minimum in QD1 and QD2. In this sense for pressures greater than the $\Gamma - X$ crossover the binding energy should increase for the impurity in QD3 and decrease for the impurity in QD2, because the expectation value of the z -distance between the impurity and the carriers decreases and increases, respectively. This behavior is clearly illustrated by the solid and dashed curves for hydrostatic pressure greater than 18 kbar; when the impurity is in QD1 (see the dotted line in the figure) the binding energy does decrease, but very gently. Figures 7c and 7d present the hydrostatic pressure dependence of the different energies associated with the terms at the right side of equation (1). The same values for the electric fields of Figures 7a and 7b were considered. For the position of the impurity it was chosen the value corresponding to the center of QD3. Notice that at $P = 0$, both E_{kinetic} and E_0 are of the order of 60 meV for $F = 0$, and of 70 meV for $F = 15$ kV/cm. For $E_{\text{confinement}}$ and $|E_{\text{Coulomb}}|$, at $F = 0$ and $P = 0$, the two energies are of the order of 5 meV and become of the order of 20 meV when $F = 15$ kV/cm. The increase of $E_{\text{confinement}}$ and $|E_{\text{Coulomb}}|$ are explained by the fact that the electric field pushes the electron wave function towards the impurity site, with two effects: (1) a decrease in the expectation value of the electron-impurity distance, therefore leading to the increase of $|E_{\text{Coulomb}}|$ and (2) a decrease of the probability of finding the electron in the QD1 and QD2 regions, and thereby causing the increasing of the probability for the barrier regions. Consequently, there will be an increase in $E_{\text{confinement}}$. On the other hand, the rise of E_{kinetic} and E_0 due to the effect of the applied electric field can be explained in terms of the shift towards higher energies of the bottom of the QD1 (see Fig. 2). It should be noticed that in the MQD system of Figure 7, the QD1 has the larger dimensions and consequently all the energies in Figure 7 are mainly associated to the QD1. By augment-

ing the hydrostatic pressure the electron mass increases and thereby both E_{kinetic} and E_0 go down (curves 1 and 2 in Fig. 7c and curve 1 in Fig. 7d). For pressures up to 13.5 kbar, the line 2 in Figure 7d shows that the E_{kinetic} has a constant behavior as a function of the hydrostatic pressure. This effect is due to: (1) the constant value of the barrier height and (2) because the applied electric field the wave function is essentially confined to the QD3. Also, for line 2 in Figure 7d, for pressures larger than 13.5 kbar the potential barriers decrease, and because the electric field the probability of finding the electron spreads over a larger region of space. This fact is consistent with the principle of uncertainty and results in a decrease in the speed of the electron, hence the dramatic decrease in kinetic energy. The rise with the hydrostatic pressure of the $|E_{\text{Coulomb}}|$ (line 4 in Fig. 7d) and the fall of $E_{\text{confinement}}$ [line 3 in Fig. 7d] are mainly due to the decrease in the height of the potential barrier. This essentially makes the electron wave function to be localized in the region of the QD3. Additionally, it should be noticed that the binding energy curves in Figures 7a and 7b follow the same behavior exhibited by $|E_{\text{Coulomb}}|$ curves in Figures 7c and 7d, respectively. Finally, we note that for zero applied electric field the absolute value of the Coulomb interaction evolves from $|E_{\text{Coulomb}}| \sim 10\%E_0$ at $P = 0$ to $|E_{\text{Coulomb}}| \sim 50\%E_0$ at $P = 30$ kbar and that for $F = 15$ kV/cm the Coulomb interaction evolves from $|E_{\text{Coulomb}}| \sim 30\%E_0$ at $P = 0$ to $|E_{\text{Coulomb}}| \sim 100\%E_0$ at $P = 30$ kbar. It means that in the present work is not possible to use, for example, perturbative methods to calculate the impurity binding energy.

In Figure 8 we present our results for the binding energy as a function of the QD length (a, c) and as a function of the barrier thickness (b, d), considering two different values of the applied electric field and two different values of hydrostatic pressure. Note that for $L_W = 0$, in both Figures 8a and 8c, our results are in agreement with those reported and discussed in Figure 5; i.e., the binding energy goes to the limit of a system confined in a $\text{Ga}_{1-x}\text{Al}_x\text{As}$ QD of radius R and length L . As soon as L_W takes on finite values, such as 10 Å, the binding energy shows a sudden jump to high values because the system is confined in three coupled QDs slightly coupled by the large barriers. From these values of L_W , the binding energy is almost insensitive to variations of L_W (with minor changes of up to 1 meV). Of course after this sudden jump the binding energy decreases because it diminishes the confinement of the carriers when the dimensions of the QD have an increment. Near the maximum limit of the length of the dots $(600 - 2 \times 45)/3 = 170$ Å it is clear that the binding energy must present a slight increase since the infinite barriers at $\pm L/2$ begin to exert their influence. Considering the effect of pressure in Figure 8a, it is clear that the binding energy must exhibit a similar behavior; however the curve (dashed line) is slightly above the solid line, which is consistent with the decreasing of the dielectric constant. Note that the dotted curve is obtained essentially by a rigid shift of the continuous curve. When we consider the effect of an electric field, Figure 8c, the results are quite similar

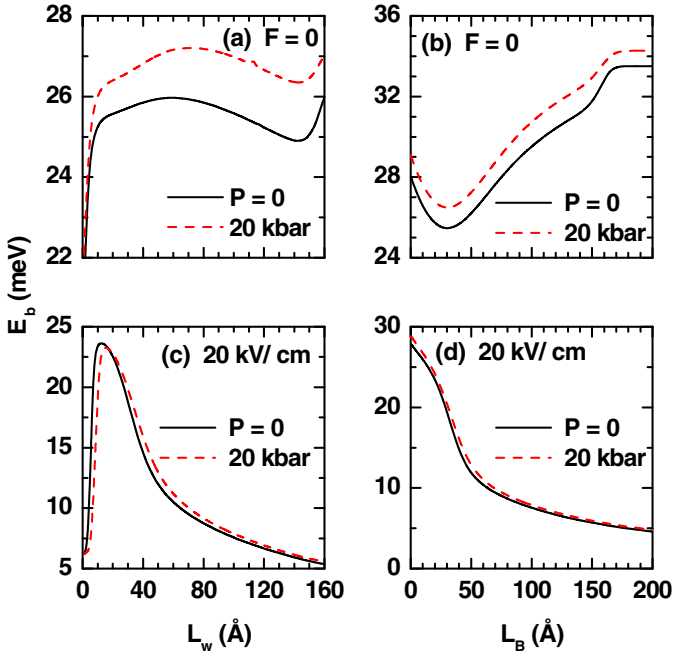


Fig. 8. (Color online) Binding energy of a donor impurity in cylindrical-shape vertically coupled GaAs-Ga_{1-x}Al_xAs MQD as a function of the dot length – L_w (a, c) and as a function of the barrier thickness – L_B (b, d). The dimensions of the structure are $(L_w, L_w, L_w, 45, 45, 100)$ Å and $(45, 45, 45, L_B, L_B, 100)$ Å with $x = 0.3$ and $z_0 = z_0^2$. In (a) and (b) $F = 0$ whereas in (c) and (d) $F = 20$ kV/cm. Solid and dashed lines are, respectively, for $P = 0$ and $P = 20$ kbar.

to those already discussed in Figure 5b, particularly for the dashed curve. Here, it is clear that the effect of the electric field is dominant over the effects of the pressure. The latter essentially translates into a rigid displacement of 5 Å towards greater lengths of QD. In Figure 8b in the limit of $L_B = 0$, the binding energy corresponds to a donor impurity in the center of a quantum dot of radius 100 Å and height 135 Å. When a finite value of L_B , such as $L_B = 20$ Å is considered, the binding energy decreases due to the augment of the expectation value of the electron-impurity distance. This is due to the fact that an important part of the probability amplitude decreases in the region of the potential barriers and increases towards the regions of the QD1 and QD3. It is important to keep in mind that in this figure the impurity is located at the center of QD2. Since $L_B = 30$ Å, the binding energy rises as long as L_B increases. The reason for this to occur is that the three QDs regions become uncoupled, with the consequent confinement of the wave function mainly in the region of QD2. Notice that from $L_B = 170$ Å the three quantum dots are completely uncoupled and the binding energy reaches the limit of an impurity in a cylindrical QD of radius 100 Å and height 45 Å. Considering now the effect of the electric field, Figure 8d, it is possible to observe that at $L_B = 0$ the curves in 8b and 8c have essentially the same binding energy value. This is explained by the fact that in a QD of height 135 Å an electric field of 20 kV/cm

is not enough to polarize the electron-impurity system. If a finite value of L_B is introduced, the probability of finding the electron in the region of QD1 and QD2 tends to zero, and is maximum in the QD3. Therefore, to enlarge the width of the barrier also increases the expected value of the electron-impurity distance and consequently the Coulomb interaction and the binding energy falls. The effects of hydrostatic pressure in Figures 8b and 8d are very similar to those observed in Figures 8a and 8c and for them are valid the same physical interpretations.

To complete the results and discussion section, we discuss below some of the limits of validity of the model we have considered. For electric fields above 150 kV/cm the electron wave function is strongly pushed towards the infinite barrier at $+L/2$ and all the structural information of the MQD of our model is lost. That value of electric field is reduced to 30 kV/cm for hydrostatic pressures around 30 kbar. This is fundamentally associated with the diminishing of the height of the potential barriers, as a result of the crossing between the Γ and X conduction bands. At 33 kbar the finite potential barriers go to zero and the system essentially reduces to a single QD of radius R and length L (approximately 600 Å in this work). For hydrostatic pressure larger than 33 kbar it occurs a semiconductor-metal transition and the system acquires an interest which is different from the one that motivates this investigation. With respect to the case of the values of the Aluminum concentration, we must emphasize that in this research we have focused on type I-heterostructures. This means heterostructures where the minimum of the conduction band and the maximum of the valence band are both in the Γ -point of the first Brillouin's zone. For this reason, the calculations reported here are restricted to consider $0 < x < 0.35$. Additionally, it is clear that in this model when $R \rightarrow \infty$ the results should reproduce those of a coupled quantum wells system. In the case of $R \rightarrow \infty$ and L large enough, our results reproduce the limits of hydrogen-like atom in the bulk, both in the case of $L_w \rightarrow 0$ with finite L_B and $L_B \rightarrow 0$ with L_w finite. The Stark effect for hydrogenic atom in the bulk is also reproduced under the above two considerations. All of the aforementioned were the limits used in this investigation to discuss the convergence of the results presented.

4 Conclusions

By using the effective mass and parabolic band approximations, a variational calculation of the shallow donor binding energy in cylindrical GaAs-Ga_{1-x}Al_xAs vertically coupled quantum dots was performed. The influence of an external electric field and applied hydrostatic pressure on this quantity is discussed for several geometries of the system. It has been found that, in general, the position of the donor atom, the applied electric field, and the hydrostatic pressure, combined with the structural dimensions of the MQD system, are critical parameters determining the value of the binding energy. The essence of this work can be stated as a predictive study about the binding energy of a donor impurity in a MQD, and our main findings can

be summarized as follow: (1) the binding energy as a function of the impurity position along the growth direction of the heterostructure follows the same behavior exhibited by the non correlated electron wave function. This means that the binding energy is symmetrical (asymmetrical) with respect to $z = 0$ for symmetrical (asymmetrical) MQD systems, with maxima in the well regions and minima in the barrier regions, (2) for increasing radius of the MQD system, the binding energy decreases and for R large enough it reaches the limit of the binding energy in a coupled QW system, (3) the binding energy increases with the augment of the Aluminum concentration in the barrier regions, (4) depending on the values of the impurity position and the structural dimensions of the MQD system (well and barrier dimensions), the electric field and the hydrostatic pressure can cause the binding energy to increase or to decrease; and finally, (5) the line-shape of the binding energy curves are mainly given by the line-shape of the Coulomb interaction. As a final conclusion we can mention that our findings confirm that both hydrostatic pressure and in-growth electric field could be suitable tools for tuning the electronic properties of multiple quantum dots, including the effect of shallow-donor impurities. We do hope this work stimulate experimental studies related to optical and electronic properties of donor impurities in vertically coupled MQD heterostructures.

This research was partially supported by Colombian Agencies: COLCIENCIAS, CODI-Universidad de Antioquia (Estrategia de Sostenibilidad Grupo de Materia Condensada-UdeA, 2009-2010), and Facultad de Ciencias Exactas y Naturales-Universidad de Antioquia (CAD-exclusive dedication project 2009-2010). Authors are grateful to Dr. M.E. Mora-Ramos for useful discussions and the critical reading of the manuscript.

References

1. S. Adachi, *J. Appl. Phys.* **58**, R1 (1985)
2. J.M. Smith, P.C. Klipstein, R. Grey, G. Hill, *Phys. Rev. B* **57**, 1740 (1998)
3. N. Dai, D. Huang, X.Q. Liu, Y.M. Mu, W. Lu, S.C. Shen, *Phys. Rev. B* **57**, 6566 (1998)
4. A. Ciucivara, B.R. Sahu, L. Kleinman, *Phys. Rev. B* **73**, 214105 (2006)
5. J. Endicott, A. Patanè, D. Maude, L. Eaves, M. Hopkinson, G. Hill, *Phys. Rev. B* **72**, R041306 (2005)
6. M. Barati, M.R.K. Vahdani, G. Rezaei, *J. Phys.: Condens. Matter* **19**, 136208 (2007)
7. A.M. Elabsy, *J. Phys.: Condens. Matter* **6**, 10025 (1994)
8. S.Y. López, N. Porrás-Montenegro, C.A. Duque, *Phys. Stat. Sol. (c)* **0**, 648 (2003)
9. A.L. Morales, A. Montes, S.Y. López, N. Raigoza, C.A. Duque, *Phys. Stat. Sol. (c)* **0**, 652 (2003)
10. C.A. Duque, S.Y. López, M.E. Mora-Ramos, *Phys. Stat. Sol. (b)* **244**, 1964 (2007)
11. M.E. Mora-Ramos, S.Y. López, C.A. Duque, *Physica E* **40**, 1212 (2008)
12. M.E. Mora-Ramos, S.Y. López, C.A. Duque, *Eur. Phys. J. B* **62**, 257 (2008)
13. J.W. González, N. Porrás-Montenegro, C.A. Duque, *Braz. J. Phys.* **36**, 944 (2006)
14. J.D. Correa, N. Porrás-Montenegro, C.A. Duque, *Braz. J. Phys.* **36**, 387 (2006)
15. E. Kasapoglu, U. Yesilgöl, H. Sari, I. Sökmen, *Physica B* **368**, 76 (2005)
16. S.G. Jayam, K. Navaneethakrishnan, *Solid State Communications* **126**, 681 (2003)
17. A.J. Peter, *Physica E* **28**, 225 (2005)
18. S.T. Pérez-Merchancano, H. Paredes-Gutierrez, J. Silva-Valencia, *J. Phys.: Condens. Matter* **19**, 026225 (2007)
19. M.G. Barseghyan, A.A. Kirakosyan, C.A. Duque, *Phys. Stat. Sol. (b)* **246**, 626 (2009)
20. M.E. Mora-Ramos, A.H. Rodríguez, S.Y. López, C.A. Duque, *PIERS Online* **4**, 263 (2008)
21. M.E. Mora-Ramos, C.A. Duque, *Braz. J. Phys.* **36**, 866 (2006)
22. M.E. Mora-Ramos, C.A. Duque, *J. Phys. Conf. Series* **167**, 012030 (2009)
23. O. Oubram, M.E. Mora-Ramos, L.M. Gaggero-Sager, *J. Phys. Conf. Series* **167**, 012031 (2009)
24. O. Oubram, M.E. Mora-Ramos, L.M. Gaggero-Sager, *Eur. Phys. J. B* **71**, 233 (2009)
25. U. Venkateswaran, M. Chandrasekhar, H.R. Chandrasekhar, T. Wolfram, R. Fischer, W.T. Masselink, H. Morkoç, *Phys. Rev. B* **31**, 4106 (1985)
26. J.H. Burnett, H.M. Cheong, W. Paul, E.S. Koteles, B. Elman, *Phys. Rev. B* **47**, 1991 (1993)
27. A.L. Morales, A. Montes, S.Y. López, C.A. Duque, *J. Phys.: Condens. Matter* **14**, 987 (2002)
28. A.L. Morales, N. Raigoza, A. Montes, N. Porrás-Montenegro, C.A. Duque, *Phys. Stat. Sol. (b)* **241**, 3224 (2004)
29. E. Kasapoglu, *Phys. Lett. A* **373**, 140 (2008)
30. Z.G. Bai, J.-J. Liu, *J. Phys.: Condens. Matter* **19**, 346218 (2007)
31. J.-J. Liu, M. Shen, S.-W. Wang, *J. Appl. Phys.* **101**, 073703 (2007)
32. A. Neogi, H. Morkoç, T. Kuroda, A. Tackeuchi, T. Kawazoe, M. Ohtsu, *Nano Lett.* **5**, 213 (2005)
33. G.J. Beirne, C. Hermannstädter, L. Wang, A. Rastelli, O.G. Schmidt, P. Michler, *Phys. Rev. Lett.* **96**, 137401 (2006)
34. H.J. Krenner, M. Sabathil, E.C. Clark, A. Kress, D. Schuh, M. Bichler, G. Abstreiter, J.J. Finley, *Phys. Rev. Lett.* **94**, 057402 (2005)
35. M. Yamagiwa, T. Mano, T. Kuroda, T. Tateno, K. Sakoda, G. Kido, N. Koguchi, F. Minami, *Appl. Phys. Lett.* **89**, 113115 (2006)
36. S. Bednarek, T. Chwiej, J. Adamowski, B. Szafran, *Phys. Rev. B* **67**, 205316 (2003)
37. B. Szafran, T. Chwiej, F.M. Peeters, S. Bednarek, J. Adamowski, B. Partoens, *Phys. Rev. B* **71**, 205316 (2005)
38. T. Chwiej, S. Bednarek, J. Adamowski, B. Szafran, F.M. Peeters, *J. Luminescence* **112**, 122 (2005)
39. B. Szafran, F.M. Peeters, S. Bednarek, *Phys. Rev. B* **75**, 115303 (2007)
40. B. Szafran, E. Barczyk, F.M. Peeters, S. Bednarek, *Phys. Rev. B* **77**, 115441 (2008)
41. J.-L. Zheng, *Physica E* **40**, 2879 (2008)
42. A. Hospodková, V. Krápek, K. Kuldová, J. Humlíček, E. Hulicius, J. Oswald, J. Pangrác, J. Zeman, *Physica E* **36**, 106 (2007)

43. L.-Z. Liu, J.-J. Liu, J. Appl. Phys. **102**, 033709 (2007)
44. W. Xie, Physica B **366**, 89 (2005)
45. J.-B. Xia, W.-J. Fan, Phys. Rev. B **40**, 8508 (1989)
46. As mentioned, here we assume the parabolic-band approximation within the effective-mass approach and note that this approximation has worked quite well in the study by Dzyubenko and Yablonskii [47] of GaAs/In_xGa_{1-x}As coupled QWs
47. A.B. Dzyubenko, A.L. Yablonskii, Phys. Rev. B **53**, 16355 (1996)
48. K. Chang, F.M. Peeters, Phys. Rev. B **63**, 153307 (2001)
49. L.P. Gorkov, I.E. Dzyaloshinskii, Soviet Physics JETP **26**, 449 (1968)
50. Yu.E. Lozovik, I.V. Ovchinnikov, S.Yu. Volkov, L.V. Butov, D.S. Chemla, Phys. Rev. B **65**, 235304 (2002)
51. A.M. Fox, D.A.B. Miller, G. Livescu, J.E. Cunningham, W.Y. Jan, Phys. Rev. B **44**, 6231 (1991)
52. I. Galbraith, G. Duggan, Phys. Rev. B **40**, 5515 (1989)
53. D.S. Chemla, J. Lumin. **30**, 502 (1985)
54. A.L. Morales, N. Raigoza, E. Reyes-Gómez, J.M. Osorio-Guillén, C.A. Duque, Superlatt. Microstruct. **45**, 590 (2009)
55. E.H. Li, Physica E **5**, 215 (2000)
56. N. Raigoza, A.L. Morales, A. Montes, N. Porras-Montenegro, C.A. Duque. Phys. Rev. B **69**, 045323 (2004)
57. D.E. Aspnes, Phys. Rev. B **14**, 5331 (1976)
58. P.Y. Yu, M. Cardona, *Fundamentals of Semiconductors* (Springer, Berlin, 1998)